Piezoresistance of Flexible Tunneling-Percolation Networks

Isaac Taylor-Harrod, Alain Nogaret*
Department of Physics, University of Bath, Bath BA2 7AY, UK

We model changes in the conductivity of flexible composite films stressed by bending. By treating stress as a perturbation of the effective medium conductivity, we obtain an expression of the piezoresistance as a function of four material parameters. The model correctly predicts resistance spikes and their recovery under the action of viscoelastic forces, in good agreement with experimental observations over stress cycles. The theory may be used to design composite materials for high sensitivity touch sensors.

I. INTRODUCTION

Systems of conducting nanoparticles embedded in flexible insulating matrices are of wide interest as materials for flexible electronics [1] and pressure sensing [2]. These materials, hereafter referred to as composites, conduct through nearest neighbor networks linked by tunneling bonds. Unlike lattice percolation systems whose conductivity is defined by local bonds and their bond occupancy probability, tunneling-percolation networks remain globally connected for any concentration of nanoparticles. In spite of a lack of percolation threshold, tunneling-percolation networks paradoxically exhibit a percolation critical conductivity $G \propto (\nu - \nu_c)^\alpha$ when the interparticle distance is of the order of the inverse tunneling length [3]. Multiple experiments have shown that the critical conductivity exponent α is not constant but increases with the nanoparticle filling fraction ν [3, 4]. Recent theoretical work [5–7] identified this departure from universality as the signature of tunneling-percolation transport. The exceptional sensitivity of electrical properties to changes in pressure is currently motivating the synthesis of novel composites [2, 4, 8–12] for making high performance sensors [11–16]. An quantitative model of the tunneling-percolation conductivity under stress is now needed to synthesize composite materials with appropriate piezoresistive properties. A piezoresistance model would further allow making constructive use of viscoelastic properties which currently limit the response time of conductive polymers [16–20].

Here we build a model of tunneling-percolation systems under stress. We treat stress as a perturbation of the effective medium conductivity [21–26] and obtain a formula for the piezoresistance which explains experimental observations over complete stress cycles. We show that step-changes in stress always increase the resistance by forming local bottlenecks in percolation paths. The rise time of the resistance is quasi-instantaneous. The magnitude of the piezoresistance increases exponentially with the amplitude of stress. Following a stress step, the resistance recovers according to a double exponential decay law which is controlled by the viscoelastic relaxation time of the network and the tunneling conductivity of local bottlenecks. The effect of material parameters controlling interparticle tunneling and viscoelastic relaxation are systematically studied. We also report on the symmetry of the piezoresistance with respect to strain reversal. In this way, we determine that the hopping rate must be independent of the orientation of tunneling bonds in spite of the presence of the electric field applied during resistance measurements [16].

The paper is organised as follows. Section I introduces the background and motivations. Section II recalls key observations from experiments on stressed composite films. Section III describes the dynamic piezoresistance model. Section IV models the dependence of the piezoresistance on material parameters. Section V discusses the results and Section VI concludes.

II. EXPERIMENTAL

Our choice of model is drawn from observations of the resistance of composites subjected to stress cycles [16] and sequences of stress steps [17, 18]. The stress protocols applied to composites of graphitic nanoparticles (HOPG) in polydimethylsiloxane (PDMS) are detailed by Chauhan et al. [16]. In this section, we recall the remarkable features of these experiments which our theory will describe.

Firstly the dependence of the d.c. conductivity on HOPG filling fraction suggests that tunneling is the interparticle conduction mechanism. The composite conductivity was found to depart from the universal power law, $G \sim (\nu - \nu_c)^\alpha$, as the critical conductivity exponent increases from 2 to 4.7 when the HOPG filling fraction increases from 24% to 32% [16]. Grimaldi and Balberg [5] have theoretically shown that this behavior may be ascribed to percolation through an extended network of nanoparticles electrically connected to one another through quantum tunneling.

Secondly, stress increments were found to give sharp increases in resistance (Fig.1(a)). The rise time is quasi-instantaneous making the changes in resistance appear as a series of spikes. The resistance spikes are always positive, whether compressive or tensile stress is applied. This is because in either case, stress temporarily disrupts the percolation network. This rectifying behavior of the piezoresistance with respect to the sign reversal

* A.R.Nogaret@bath.ac.uk

of stress is similar to that observed in crystalline silicon ribbons [27, 28].

Thirdly, following each stress step, the percolation network relaxes into a new state of equilibrium driven by viscoelastic forces (Fig.1(a)). During this relaxation phase, the resistance recovers according to a double exponential dependence on time (Fig.1(b)). This behavior has been reported in other composite systems incorporating carbon nanotubes [17] and graphene [18]. The double exponential recovery of the resistance validates quantum tunneling as the inter-particle conduction mechanism. This is because the first exponential describes the dependence of bond conductivity on tunneling barrier width. The second exponential describes the viscoelastic relaxation of the tunneling barrier width on the time scale of the polymer creep time. The double exponential decay was observed in each step of a stress cycle (Fig.1(b)) and over a range of filling fractions [16] hence was very robust.

III. MODEL

A. Stress and strain in the composite film

The composite is modelled as an isotropic medium of hard conductive spheres of diameter d randomly dispersed in a soft polymer matrix (Fig.2). We begin by calculating the stresses and strains in the bent bilayer (Fig.2). The bilayer consists of a thin composite film of thickness a_c fabricated on a flexible substrate of thickness a_s. By changing the radius of curvature of the substrate (ρ), the composite was subjected to cycles of compressive and tensile stress. This method presents several advantages. Stress is distributed uniformly in the plane of the bilayer. The biaxial stress $(\sigma_{xx}(t), \sigma_{yy}(t), 0)$ only depends on ρ and material parameters, hence may be calculated accurately. The stress direction may be reversed by loading or unloading the composite. The magnitude of the stress may be controlled by the size of step changes in curvature radius. To model experiments, we consider stress cycles consisting of N decreases in curvature radius (stress loading) followed by N increases in curvature radius (stress unloading). The time interval between stress steps is τ.

At time $t = n\tau$, the curvature radius changes from $\rho_{n-1} \to \rho_n$. Balancing the forces and torques in the bilayer [29] gives the stress increment in the composite as:

$$\begin{cases} \Delta_n \sigma_{xx} = \dfrac{E_s a_s^3}{6(1-\gamma_s^2) a_c (a_c + a_s)} \Delta_n (1/\rho) \\ \Delta_n \sigma_{yy} = \dfrac{E_s a_s^3 \gamma_s}{6(1-\gamma_s^2) a_c (a_c + a_s)} \Delta_n (1/\rho) \\ \Delta_n \sigma_{zz} = 0 \end{cases}, \qquad (1)$$

where $\Delta_n(1/\rho) = 1/\rho_n - 1/\rho_{n-1}$; E_s and γ_s are respectively the Young's modulus and the Poisson ratio of the substrate.

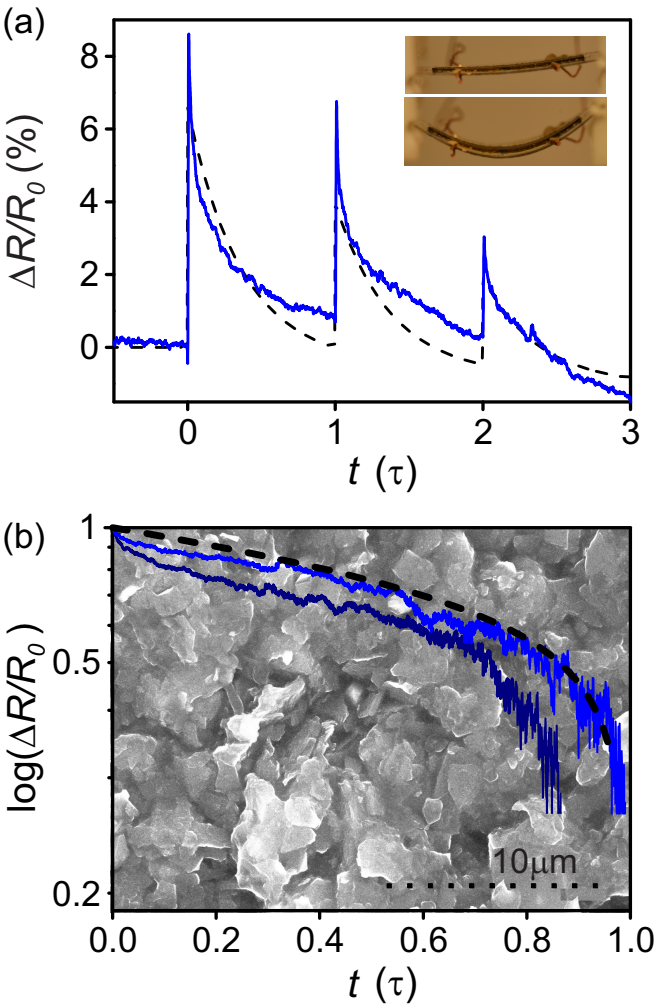

FIG. 1. *(color online)* (a) Resistance of a HOPG/PDMS composite film compressed at time intervals of $\tau = 200s$: experiment (full line) and theory (dashed line). Inset: the composite is stressed by bending the acetate substrate on which it is fabricated; (b) The resistance recovery between two stress increments follows a double exponential decay law. The piezoresistance (full lines) is normalized at the start of each time interval. The dashed line was calculated with Eq.22 and parameters: $\tau_c = 180s$, $\epsilon\tau_c/\tau_R = 0.1$, $\nu_0 = 31\%$ (see text). Background image: SEM of the HOPG/PDMS composite.

In the time interval $n\tau < t < (n+1)\tau$ following the stress increment, stress relaxes through viscoelastic deformation of the polymer matrix. This relaxation is in general incomplete as viscoelastic solids are known to retain a fraction $0 < \epsilon < 1$ of the applied stress at long times [30]. The stress accumulated in the composite at time t may therefore be written:

$$\sigma_{\alpha\alpha}(t) = \sum_{n=0}^{2N-1} \Delta_n \sigma_{\alpha\alpha}\, H(t - n\tau) \left[(1-\epsilon) e^{-\frac{t-n\tau}{\tau_R}} + \epsilon \right], \qquad (2)$$

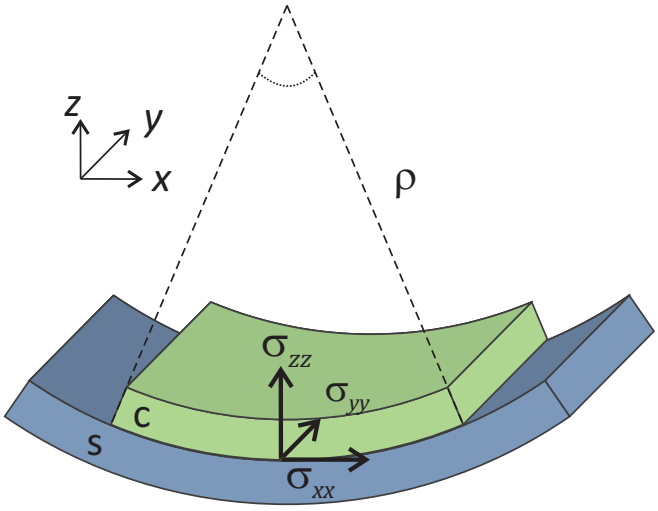

FIG. 2. *(color online)* The composite layer (c) is stressed by bending the flexible substrate (s). The stress in the composite (σ) only depends on the curvature radius ρ and material parameters. For a cellulose acetate substrate and a HOPG/PDMS composite, material parameters are: Young's moduli $E_s = 41 \pm 11$MPa, $E_c = 1.8 \pm 0.05$MPa; Poisson ratios $\gamma_s = 0.391 \pm 0.008$ $\gamma_c = 0.391 \pm 0.008$; and layer thicknesses $a_c = a_s = 100\mu$m.

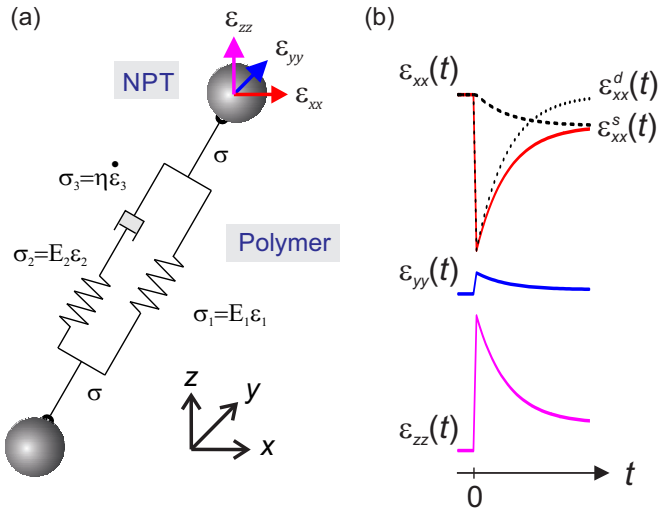

FIG. 3. *(color online)* (a) Linear viscoelastic model of the polymer matrix. E_1 and E_2 are the partial Young moduli. η is the polymer viscosity. This model yields the stress relaxation time $\tau_R = \eta E_2^{-1}$ and the strain relaxation time (creep time) $\tau_c = \eta(E_1^{-1} + E_2^{-1})$. (b) Time evolution of the principal strain components after the curvature radius is decreased at $t = 0$ (full lines). Each strain component is the sum of a static part (dashed lines) which tends to a finite value, and a dynamic part (dotted lines) which vanishes.

where $H(t)$ is the Heavyside step function, $\alpha, \beta \equiv \{x, y, z\}$, $\Delta\sigma_{\alpha\alpha}$ are the stress steps given by Eq.1 and τ_R is the stress relaxation time (see below). The incremental nature of changes in curvature radius makes the calculation of the induced strain easier to perform using Laplace transforms:

$$\begin{aligned} \bar{\sigma}_{\alpha\beta}(p) &= \int_0^\infty dt\ \sigma_{\alpha\beta}(t)\, e^{-pt} \\ \bar{\varepsilon}_{\alpha\beta}(p) &= \int_0^\infty dt\ \varepsilon_{\alpha\beta}(t)\, e^{-pt} \end{aligned} \quad , \tag{3}$$

The strain tensor is diagonal due to the isotropic nature of the composite. Its principal components are given by the three dimensional Hooke's law [30]. Hunter [30] has further shown that Hooke's law holds true for the linear viscoelastic solid whose viscoelastic time constants are accounted for in Laplace transforms. The principal strain components are:

$$\begin{pmatrix} \bar{\varepsilon}_{xx}(p) \\ \bar{\varepsilon}_{yy}(p) \\ \bar{\varepsilon}_{zz}(p) \end{pmatrix} = \frac{1}{\bar{E}(p)} \begin{pmatrix} 1 & -\gamma_c & -\gamma_c \\ -\gamma_c & 1 & -\gamma_c \\ -\gamma_c & -\gamma_c & 1 \end{pmatrix} \begin{pmatrix} \bar{\sigma}_{xx}(p) \\ \bar{\sigma}_{yy}(p) \\ \bar{\sigma}_{zz}(p) \end{pmatrix} , \tag{4}$$

where $\bar{E}(p)$ is the viscoelastic Young's modulus of a single percolation bond. Using Eqs.1 and 2, one may write the strain components as a function of the driving force:

$$\begin{cases} \bar{\varepsilon}_{xx}(p) = \dfrac{1 - \gamma_c\gamma_s}{\bar{E}(p)} \bar{\sigma}_{xx}(p) \\ \bar{\varepsilon}_{yy}(p) = \dfrac{\gamma_s - \gamma_c}{\bar{E}(p)} \bar{\sigma}_{xx}(p) \\ \bar{\varepsilon}_{zz}(p) = \dfrac{-\gamma_c(1 + \gamma_s)}{\bar{E}(p)} \bar{\sigma}_{xx}(p) \end{cases} . \tag{5}$$

We then calculate the viscoelastic modulus $\bar{E}(p)$, by modeling the polymer layer separating two nanoparticles (NPT) with the spring-dashpot link shown in Fig.3(a). In this model, E_1 and E_2 are the partial Young moduli and η is the polymer viscosity. The study of the linear response regime is justified by the infinitesimally small strain increments applied with each bend ($< 0.5\%$). The relationship between stress (σ) and strain (ε) across nanoparticles is then obtained by solving the spring-dashpot model of Fig.3(a):

$$\dot{\sigma} + \frac{\sigma}{\tau_R} = E_D \left(\dot{\varepsilon} + \frac{\varepsilon}{\tau_c} \right) , \tag{6}$$

where $E_D = E_1 + E_2$ is the dynamic Young's modulus, $\tau_R = \eta/E_2$ is the stress relaxation time and $\tau_c = \eta(E_1 + E_2)/(E_1 E_2)$ is the strain relaxation time (or creep time). Taking the Laplace transform of Eq.6 gives the viscoelastic Hooke's law of individual percolation bonds:

$$\bar{E}(p) = \frac{\bar{\sigma}(p)}{\bar{\varepsilon}(p)} = E_D \frac{p + \tau_c^{-1}}{p + \tau_R^{-1}} . \tag{7}$$

The strain dynamics in the time domain follows from taking the the inverse Laplace transform of Eq.7:

$$\varepsilon(t) = E_D^{-1}\left[\sigma(t) + \int_{-\infty}^{t} \Psi(t-t')\frac{d\sigma(t')}{dt'}dt'\right], \quad (8)$$

where

$$\Psi(t) = \left(\frac{\tau_c}{\tau_R}\right)\left[1 - \exp\left(-\frac{t}{\tau_c}\right)\right] \quad . \quad (9)$$

The first term in Eq.8 describes the elastic response to stress. This explains that strain increases instantaneously following a stress step (Fig.3(b)). The second term is the hereditary integral which contains the memory of earlier changes in stress weighted by the creep function $\Psi(t)$. This second term explains the viscoelastic relaxation of strain after a stress step. Note that the 1D Hooke's law (Eq.7) only differs from the 3D Hooke's law (Eq.5) by a constant multiplicative term. Therefore the 3D strain components will follow the dynamics prescribed by Eq.8. Inserting the stress components of Eqs.1 and 2 into Eq.8 yields the following expression for the 3D strain in the composite. This strain may be decomposed as the sum of a *dynamic* strain, $\boldsymbol{\varepsilon}^d$:

$$\begin{cases} \varepsilon^d_{xx}(t) = -\dfrac{E_s}{6E_c}\dfrac{1-\gamma_c\gamma_s}{1-\gamma_s^2}\dfrac{a_s^3}{a_c(a_c+a_s)}\, f(t,N) \\ \varepsilon^d_{yy}(t) = -\dfrac{E_s}{6E_c}\dfrac{\gamma_s-\gamma_c}{1-\gamma_s^2}\dfrac{a_s^3}{a_c(a_c+a_s)}\, f(t,N) \\ \varepsilon^d_{zz}(t) = +\dfrac{E_s}{6E_c}\dfrac{\gamma_c(1+\gamma_s)}{1-\gamma_s^2}\dfrac{a_s^3}{a_c(a_c+a_s)}\, f(t,N) \end{cases} , \quad (10)$$

where

$$f(t,N) = \sum_{n=0}^{2N-1} \Delta_n(1/\rho)\, H(t-n\tau) e^{-\frac{t-n\tau}{\tau_c}} \quad , \quad (11)$$

and a *static* strain, $\boldsymbol{\varepsilon}^s$:

$$\begin{cases} \varepsilon^s_{xx}(t) = -\dfrac{E_s}{6E_c}\dfrac{1-\gamma_c\gamma_s}{1-\gamma_s^2}\dfrac{a_s^3}{a_c(a_c+a_s)}\, g(t,N) \\ \varepsilon^s_{yy}(t) = -\dfrac{E_s}{6E_c}\dfrac{\gamma_s-\gamma_c}{1-\gamma_s^2}\dfrac{a_s^3}{a_c(a_c+a_s)}\, g(t,N) \\ \varepsilon^s_{zz}(t) = +\dfrac{E_s}{6E_c}\dfrac{\gamma_c(1+\gamma_s)}{1-\gamma_s^2}\dfrac{a_s^3}{a_c(a_c+a_s)}\, g(t,N) \end{cases} , \quad (12)$$

where

$$g(t,N) = \sum_{n=0}^{2N-1} \Delta_n(1/\rho)\, H(t-n\tau)\epsilon\frac{\tau_c}{\tau_R}\left(1 - e^{-\frac{t-n\tau}{\tau_c}}\right). \quad (13)$$

$\boldsymbol{\varepsilon}^d(t)$ is a transient strain which vanishes at long times whereas $\boldsymbol{\varepsilon}^s(t)$ is driven by stress accumulation and remains finite. The latter strain tends towards a finite value which is proportional to the incomplete stress relaxation ratio ϵ. The time evolution of the principal strain components following a decrease in curvature radius is shown in Fig.3(b). The composite contracts in the x-direction ($\varepsilon_{xx} < 0$) while it expands in the z-direction ($\varepsilon_{zz} > 0$). The residual expansion in the y-direction arises from differences in Poisson ratios between the substrate and the composite ($\gamma_s < \gamma_c$). The strain changes sign when the curvature radius is increased instead. Stress cycles therefore allow studying the symmetry of the piezoresistance with respect to change in the sign of strain. Throughout a cycle, deformation occurs at constant volume, $\varepsilon_{xx} + \varepsilon_{yy} + \varepsilon_{zz} = 0$, only if the polymer matrix is a perfect elastomer: $\gamma_c = 0.5$.

B. EMA average conductivity and bond length

In the steady state, the conductivities of tunneling bonds follow a distribution [7] centered on the average bond conductivity g_0. This conductivity is the conductivity of the occupied bonds in the lattice percolation network equivalent to the actual tunnelling-percolation system. g_0 is calculated within the Effective Medium Approximation (EMA) [5]. From g_0, one will infer the average tunneling barrier width b_0 between nearest neighbors which one will compare to the average interparticle distance $\bar{b}$. We first consider the nearest neighbor probability distribution function (three dimensional), $P(b)$, for hard spheres of radius d randomly dispersed in the polymer matrix [31, 32]:

$$P(b) = \frac{24\nu(\gamma_1 x^2 + \gamma_2 x + \gamma_3)}{d}\exp\left[-8\nu\gamma_1(x^3-1) - 12\nu\gamma_2(x^2-1) - 24\nu\gamma_3(x-1)\right], \quad (14)$$

where ν is the volume fraction of conductive nanoparticles, $x \equiv 1 + b/d$ and $\gamma_1 = (1+\nu)/(1-\nu)^3$, $\gamma_2 = -(\nu/2)(\nu+3)/(1-\nu)^3$ and $\gamma_3 = (1/2)\nu^2/(1-\nu)^3$. The average tunneling gap between neighboring spheres is $\bar{b} = \int_0^\infty db\, bP(b)$. In the range of filling fractions $24\% < \nu < 32\%$, this interparticle distance is approximated (to within a few percents) by $\bar{b} \approx d/4\left[(\pi/6\nu)^{1/3} - 1\right]$ [4]. For HOPG nanoparticles of 450nm diameter [16], the average interparticle distance thus varies from 20nm to 34nm as ν decreases from 32% to 24%. Filling fractions in this range are the most relevant to experiments because 32% is the miscibility threshold of HOPG nanoparticles in PDMS whereas 24% is the percolation threshold ν_c [4].

We next calculate the average separation of conductive nanoparticles b_0 by calculating the average EMA conductivity of a 3D tunneling-percolation network [5, 7]:

$$\int_0^\infty db\frac{P(b)}{g(b)+2g_0} = \frac{p-p_c}{2g_0 p} \, . \quad (15)$$

Here p is the bond occupancy probability corresponding to filling fraction ν. Given that the critical filling fraction $\nu_c = 24\%$ is not vanishingly small, one may solve Eq.15 to a good approximation by substituting $(p - p_c)/p$ with $(\nu - \nu_c)/\nu$ [5].

The tunnel conductivity $g(b)$ between neighboring spheres was calculated by recalling the tunnel current density through a rectangular barrier [33, 34]:

$$J(b) = \frac{3}{4\pi} G_0 \kappa \frac{e^{-2\kappa b}}{b} V \ , \qquad (16)$$

where $G_0 = 2e^2/h$ is the quantum conductance and $\kappa = \sqrt{2mV_0}/\hbar$ is the inverse of the tunnel decay length through the potential barrier of height V_0 and width b. The tunnel current between hard spheres was calculated by integrating Eq.16 over the cross sectional area (inset Fig.4):

$$I = \int_0^{2\pi} d\phi \int_0^{\pi/2} d\theta \, (d/2)^2 \sin\theta \cos\theta \, J(s(\theta)) \qquad (17)$$

where $s(\theta) = b + d(1 - \cos\theta)$ is the tunnel gap at angle θ relative to the symmetry axis. After some algebra, one obtains the bond conductivity as:

$$g(b) = \frac{3}{16} G_0 \left(u_T \int_{u_L}^{u_T} du \frac{e^{-u}}{u} + e^{-u_T} - e^{-u_L} \right), \qquad (18)$$

where $u_L = 2\kappa b$ and $u_T = u_L + 2\kappa d$. The conductivity of a tunnel bond is plotted in Fig.4 as a function of the tunnel barrier width. We then used Eq.18 in Eq.15 to calculate the EMA conductivity g_0 at three filling fractions ν_0 =26%, 28% and 30%. The EMA tunnel barriers b_0 are read on the horizontal axis of Fig.4 for each ν_0. We find κb_0 =11.1 (30%), 14 (28%) and 20.2 (26%). The tunnel barriers of conducting bonds are on average shorter than the average interparticle distance calculated from the filling fraction $\kappa\bar{b}$ =17.2 (30%), 19.6 (28%) and 22.2 (26%). In the next section, we construct a perturbative model of the EMA conductivity, by assuming percolation bonds have initial length b_0 and conductivity g_0.

C. Perturbative piezoresistance model

One now calculates the effect of infinitesimal strain on the conductivity of the composite initially at rest. A step change in strain will change the inter-particle distance $b_0 \to b + \Delta b_{kl}$ where b is the new mean interparticle distance and Δb_{kl} is the relative change in length of bond k of percolation line l. An infinitesimal strain ($< 0.5\%$) allows us in first approximation to neglect the re-routing of percolation paths. We also assume that all conducting bonds have similar length $b_{kl} \simeq b_0$ prior to the application of stress. One may then apply Kirchhoff current

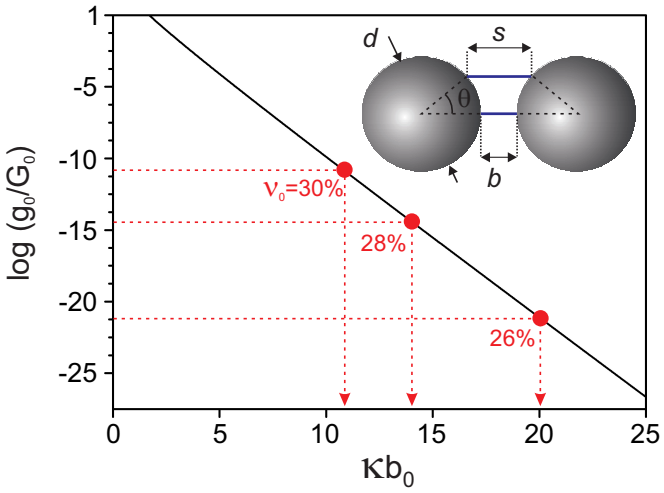

FIG. 4. Conductivity of a percolation bond (normalized by the quantum conductance) as a function of the tunneling barrier width. The EMA average conductivity was calculated for three nanoparticle filling fractions (dots). The corresponding interparticle distances are indicated on the horizontal axis. Inset: Inter-particle tunneling model. Parameters: $\kappa = 0.75\text{nm}^{-1}$, d=200nm.

and voltage laws to L percolation lines running in parallel across the composite. Assuming each of these lines contains K bonds, the conductivity of the composite is:

$$G = \sum_{l=1}^{L} \frac{b_0^{-1} \exp(2\kappa b_0)}{\sum_{k=1}^{K} b_{kl}^{-1} \exp(2\kappa b_{kl})} g_0(b_0), \qquad (19)$$

where $g_0(b_0)$ is the EMA conductivity in the initial state. Making the substitution $b_0 \to b + \Delta b_{kl}$ into Eq.19 and retaining the first order terms in $\Delta b_{kl}/b_0$, we obtain the conductivity to first order in strain as the product of two terms:

$$G = G_s(b) \Gamma_d \ . \qquad (20)$$

Here $G_s(b) = (L/K) g_0(b)$ is the baseline conductivity of the composite determined by the new average interparticle distance b. Γ_d is a dimensionless term which describes the transient dynamics:

$$\Gamma_d = \frac{1}{L} \sum_{l=1}^{L} \frac{1}{\frac{1}{K} \sum_{k=1}^{K} \exp\left(2\kappa b \frac{\Delta b_{kl}}{b}\right)} \ . \qquad (21)$$

To calculate Eq.21, one notes that composite films used in experiments [16] are several orders of magnitude longer than the average percolation bond, $d + b \approx 600$nm. Each percolation path will therefore include at least $K \sim 10^4$ bonds. This large number allows substituting the discrete

sum over k with a continuous integral over the 4π solid angle. The resistance of the composite is given by:

$$R(t) = \frac{R_s(b)}{4\pi}\int_0^{2\pi} d\phi \int_0^{\pi} d\theta \sin\theta e^{2\kappa b\frac{\Delta b(\theta,\phi,t)}{b}} w(\theta,\phi) \tag{22}$$

where $R_s(b) = 1/G_s(b)$ and $w(\theta,\phi)$ is a weight function we describe below. The magnitude of a change in bond length $\Delta b(\theta,\phi)$ depends on the orientation of this bond in the dynamic strain through:

$$\begin{aligned}\frac{\Delta b(\theta,\phi,t)}{b} &= \frac{\sqrt{\sum\limits_{\alpha=x,y,z}(b_\alpha+\Delta b_\alpha)^2}-b}{b}, \\ &\simeq \boldsymbol{n}^T\boldsymbol{\varepsilon}^d(t)\,\boldsymbol{n}\end{aligned} \tag{23}$$

where $\boldsymbol{n} \equiv (\sin\theta\cos\phi, \sin\theta\sin\phi, \cos\theta)$ is the unit vector and $\boldsymbol{\varepsilon}^d$(t) the dynamic strain tensor whose principal components are given in Eq.10. The weight function $w(\theta,\phi)$ describes the anisotropy of the hopping rate. This allows modeling different scenarios of anisotropic conduction. For example, $w(\theta,\phi) = 1$ assumes equally probable hopping in all directions. $w(\theta,\phi) = 2\sin\theta \mid \cos\phi \mid$ assigns a greater weight to the hopping probability in the x-direction to model the electric field applied during resistance measurements.

We now calculate the change in baseline resistance $R_s(b)$. R_s is the inverse of the static conductivity of the composite, $G_s \sim (\nu-\nu_c)^\alpha$. One proceeds by relating the change in tunnelling barrier width $b_0 \to b = b_0(1+\varepsilon^s_{xx})$ to a virtual change in filling fraction $\nu_0 \to \nu$. This is done through the relationship $b \simeq d/4\left[(\pi/6\nu)^{1/3}-1\right]$ [4] between the average barrier width and the filling fraction. We calculate the new effective filling fraction to be:

$$\nu \simeq \nu_0\left[1 - 12\frac{b_0/d}{1+4b_0/d}\varepsilon^s_{xx}\right]. \tag{24}$$

ν is then inserted in the conductivity to obtain its dependence on the static strain:

$$G_s(\nu) \simeq G_s(\nu_0)\left(1 - 12\frac{\nu_0}{\nu_0-\nu_c}\frac{b_0/d}{1+4b_0/d}\alpha\varepsilon^s_{xx}\right), \tag{25}$$

One may rewrite this result as a function of ν_0 only by substituting in $b_0 = d/4\left[(\pi/6\nu_0)^{1/3}-1\right]$ into Eq.25. The steady state resistance normalized by the initial resistance follows as:

$$\frac{R_s(b)}{R_s(b_0)} = 1 + 3\frac{\nu_0}{\nu_0-\nu_c}\left(1-\left[\frac{6\nu_0}{\pi}\right]^{1/3}\right)\alpha\varepsilon^s_{xx}(t). \tag{26}$$

Eq.26 predicts a linear dependence of the baseline resistance on stress. This prediction is in very good agreement with observations in Fig.6(d) when stress is either loaded or unloaded. Eq.26 predicts that the rate of change of the resistance baseline becomes increasingly steep as ν_0 approaches the critical filling fraction ν_c.

IV. RESULTS

A. Random vs directional hopping

Percolation bonds which are aligned with the tensile component of strain will be elongated and form resistance bottlenecks. In contrast, bonds which are aligned with the compressive component of strain will become more conductive. The directions of compression and elongation will be swapped if the curvature radius is increased instead. This section investigates the symmetry of the piezoresistance over cycles in which the strain changes sign. We show that any asymmetry in the piezoresistance implies that the hopping rate is directed preferentially towards one direction.

Resistance spikes are generated through the interplay of percolation-tunneling and the 3D strain field. Decreasing the curvature radius has the effect of elongating percolation bonds in the z (and y) directions (Fig.3(b)). These bonds become the weak links in the chain as their resistance increases exponentially. This rapidly leads to the formation of resistance bottlenecks which determine the overall resistance of percolation lines. The increase in resistance happens instantly through the elastic coupling term in Eq.8. Bonds oriented in the x direction will instead be compressed. Their contribution to the resistance under the integral of Eq.23 will decrease exponentially. This picture describes well the first 10 spikes induced by stress loading in Fig.5(a). Between spikes the percolation network relaxes towards a new steady state.

The following 10 resistance spikes in Fig.5(a) occur as stress unloading returns the composite to its flat state. Bonds oriented in the x direction are now elongated and are responsible for the resistance spikes. By assuming an isotropic hopping rate ($w(\theta,\phi) = 1$), our model predicts resistance spikes which are symmetric with respect to stress loading and unloading. In other words, resistance bottlenecks formed at different locations and with different orientations increase the resistance by the same amount. This scenario matches experimental observations [16].

If instead one assumes preferential hopping in one direction, the model predicts a strongly asymmetrical piezoresistance over a stress cycle. Fig.5(b) models hopping directed by the measurement electric field. In this case, x-oriented bonds to control the resistance. During the loading phase compression of the x-oriented bonds gives *negative* resistance spikes. During the unloading phase, these bonds expand giving positive resistance spikes. The positive spikes in the second half of panel (b) have greater amplitude than the equivalent spikes in panel (a) because the resistance increases in the x-direction are not compensated by the shortening of bonds in the z-direction.

The observation of symmetric loading-unloading cycles in all experiments [16] indicates that the hopping rate is isotropic.

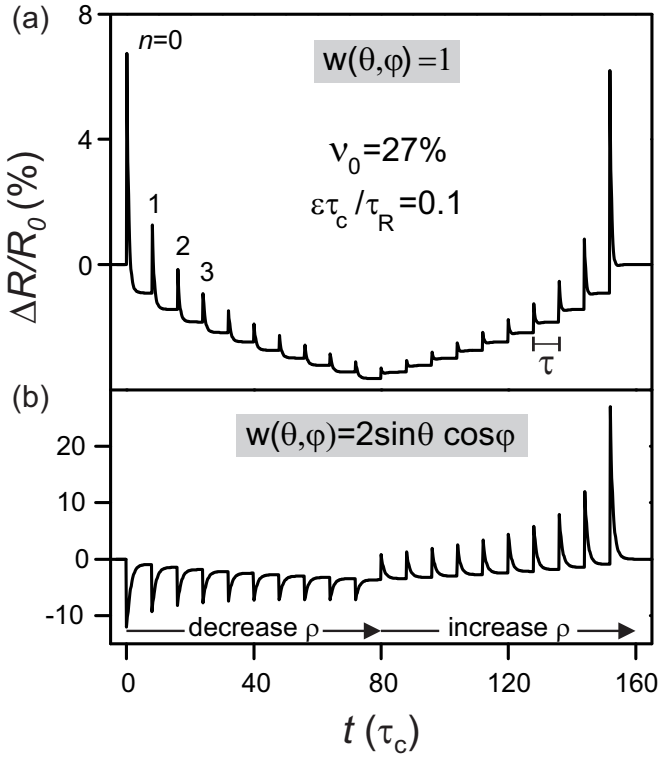

FIG. 5. *(color online)* Time dependence of the piezoresistance over a loading-unloading cycle calculated by assuming (a) an equal hopping probability in all directions (b) hopping driven by the electric field. Parameters: $\kappa = 0.75\text{nm}^{-1}$, $\tau = 5\tau_c$, $\epsilon = 0.1$, $\nu_0 = 27\%$.

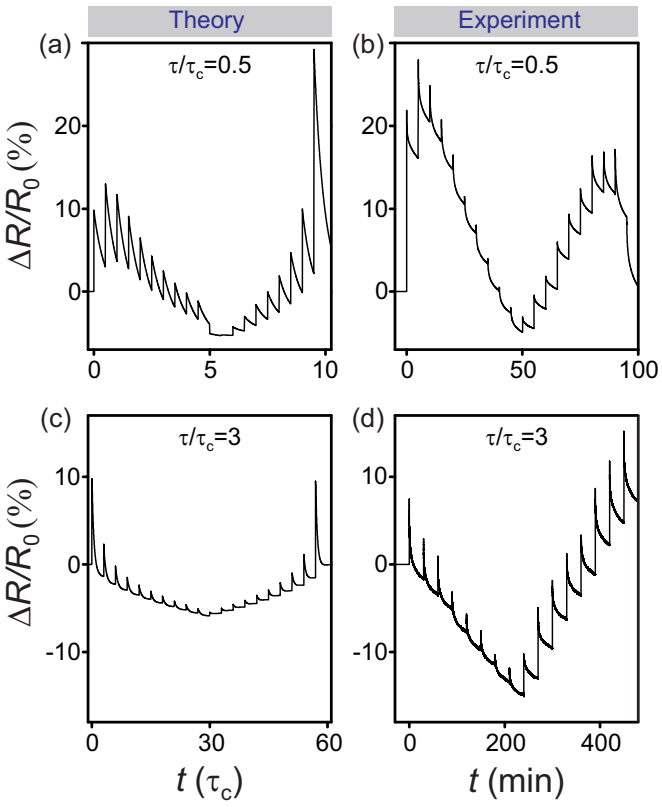

FIG. 6. Viscoelastic memory of the composite over a stress cycle. When $\tau < \tau_c$ the piezoresistance exhibit a M-shape profile (a) theory, (b) experiment. Intervals between stress steps are too short for complete stress relaxation. When $\tau > \tau_c$ the piezoresistance exhibit a V-shape profile (c) theory, (d) experiment.

B. Dependence on material parameters

We now model the effect of material parameters on the piezoresistance. We model the change in resistance over a cycle of 10 loading and 10 unloading stress steps.

The viscoelastic memory of the composite film was probed by varying the duration of stress steps τ relative to the viscoelastic creep time τ_c. When $\tau = 0.5\tau_c$, incomplete relaxation between stress steps produces a M-shaped piezoresistance (Fig.6(a)) which is in qualitative agreement with experiment (Fig.6(b)). In contrast when time intervals between bends are sufficient to allow complete stress relaxation, the resistance profile evolves towards a V-shaped pattern. This transition from M- to V-shaped resistance profile is predicted in Fig.6(c) for $\tau = 3\tau_c$ and is observed experimentally in Fig.6(d).

The resistance dependence on ν_0 is shown in Fig.7. Decreasing ν_0 from 30% to 26% increases the amplitude of resistance spikes relative to the baseline. This may be explained by the widening of tunnel barriers at lower filling fractions with the consequence that the same amount of strain produces a greater absolute change in barrier width hence resistance spikes of greater amplitude. Decreasing ν_0 also makes the baseline resistance drop at a steeper rate. This is because the strain prefactor in Eq.26 diverges when ν_0 approaches the critical filling fraction.

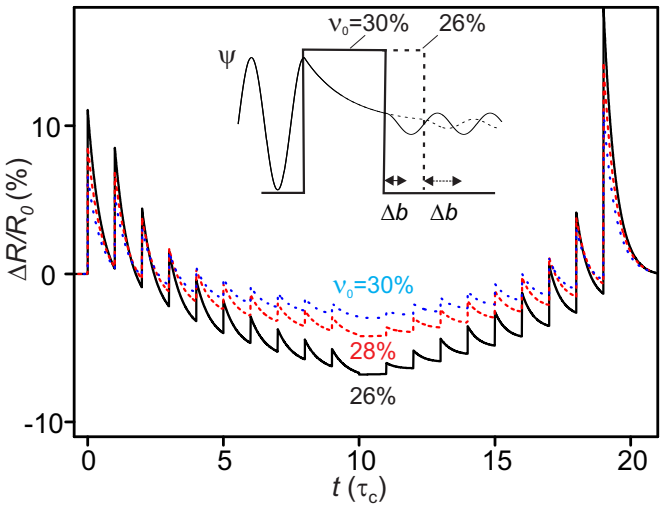

FIG. 7. *(color online)* Resistance calculated over a loading-unloading cycle for three different filling fractions $\nu_0 = 26\%$, 28% and 30%. Inset: the inter-particle tunnel barrier corresponding to two filling fractions. The wider the tunnel barrier, the greater the stress induced increase in resistance. Parameters: $\kappa = 0.75\text{nm}^{-1}$, $\tau = \tau_c$, $\epsilon = 0.1$.

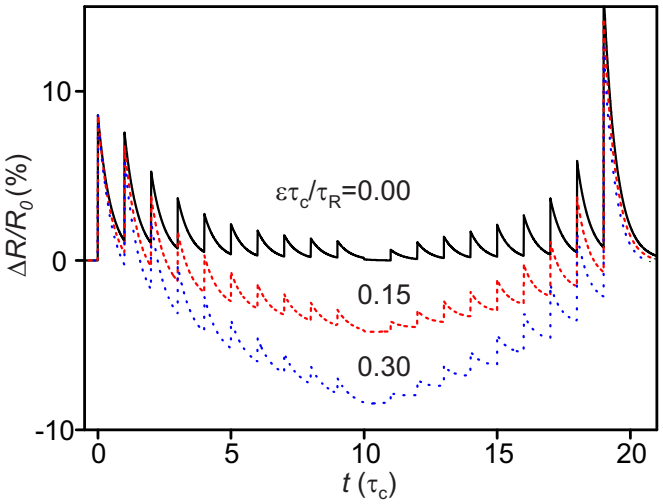

FIG. 8. *(color online)* Resistance calculated over a loading-unloading cycle for three values of the incomplete relaxation parameter $\epsilon\frac{\tau_c}{\tau_R}$ = 0,0.15 and 0.30. Parameters: κ = 0.75nm^{-1}, $\tau = \tau_c$, $\epsilon = 0.1$, $\nu_0 = 28\%$.

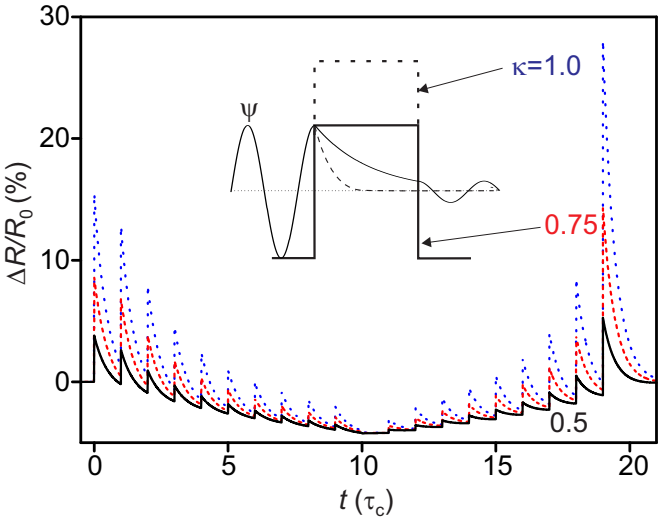

FIG. 9. *(color online)* Resistance calculated over a loading-unloading cycle for three values of the inverse tunnel length: κ = 0.5, 0.75 and 1.0nm^{-1}. Parameters: $\tau = \tau_c$, $\epsilon = 0.1$, $\nu_0 = 28\%$.

The effect of incomplete stress relaxation (ϵ) in the composite is studied through the variation of the dimensionless parameter $\epsilon\frac{\tau_c}{\tau_R}$ which appears in Eq.13. The effect of increasing this parameter from 0% to 30% is shown in Fig.8. This parameter has no effect on the amplitude of resistance spikes. However, the baseline resistance drops at a steeper rate when ϵ increases. This is because incomplete recovery leading to greater stress accumulation reduces the inter-particle distances with each compressive step.

Fig.9 plots the theoretical resistance over a stress cycle for three different values of the polymer-nanoparticle band offset, V_0. The curves are parameterized by the inverse tunnel length κ = 0.5, 0.75 and 1.0nm^{-1}. Increasing the tunneling barrier height exponentially increases the magnitude of piezoresistance spikes. Greater sensitivity to stress will therefore be achieved by choosing filler/matrix materials with large band offset. The band offset has no effect on the resistance baseline.

C. Piezoresistance

Fig.10 plots the piezoresistance as a function of the magnitude of strain. The piezoresistance is defined as the height of the first resistance spike in the stress cycle (inset). The full lines show the theoretical piezoresistance calculated from Eq.22 for different values of the band offset. This piezoresistance increases exponentially with strain. Minute changes in strain (<0.5%) give piezoresistance considerably larger than that of inorganic crystal [35–38]. The curves are calculated for different band offsets V_0. They demonstrate that a composite sensitivity to stress may be increased by choosing a large band offset for the nanoparticle/polymer system. The piezoresistance data measured on two HOPG/PDMS composites are shown by the square and dots symbols. The line of best fit corresponds to a HOPG/PDMS tunnelling barrier of $V_0 \approx 0.3$eV.

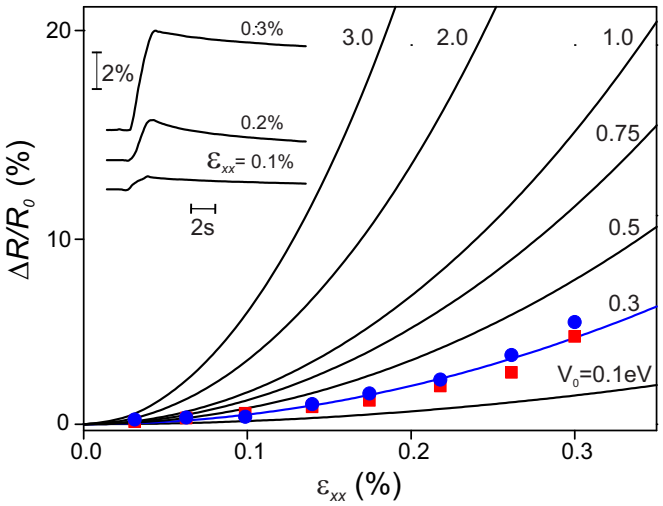

FIG. 10. *(color online)* Dependence of the piezoresistance on the magnitude of strain (full lines) calculated for different values of the band offset V_0 of hypothetical nanoparticle/polymer material systems. The piezoresistance of the PDMS/HOPG system (symbols) was measured on two composites with filling fraction ν_0=28%. Inset: amplitude of the first resistance spike measured as a function of strain (experiment).

V. DISCUSSION

Our theoretical model relies on four phenomenological parameters: the filling fraction of conductive nanoparti-

cles, ν_0; the band offset between the polymer matrix and nanoparticles, V_0; the incomplete stress relaxation ratio of the non-ideal viscoelastic solid, ϵ; and the viscoelastic creep time, τ_c. Parameters ϵ and ν_0 determine the rate of change of the resistance baseline with strain. Parameters ν_0 and V_0 determine the sensitivity of the material to stress through the piezoresistance. Parameter τ_c is the time constant of the double exponential decay (Fig.1(b)).

We justify our perturbative approach by observing that minute amounts of strain are sufficient to induce significant increases in resistance. Our phenomenological model accounts for most experimental features. The sharp rise in resistance at each stress step (dashed lines, Fig.1(a)) is due to the instantaneous disruption of the percolation network by the tensile component of strain. This is the ε^d_{zz} component when ρ decreases and ε^d_{xx} when ρ increases. Eq.22 correctly describes the double exponential decay of the experimental resistance in Fig.1(b) (dashed lines). This decay arises from viscoelastic relaxation of conductivity through tunnel bottlenecks. The theory correctly predicts the rectifying behaviour of the resistance with respect to the change in sign of strain. This is observed as positive resistance spikes when stress is loaded or unloaded. We have seen that this rectifying behavior implies that the hopping rate must be isotropic. Here strain is an experimental parameter which provides useful new insight into microscopic percolation processes. The theory successfully describes viscoelastic memory effects in the resistance (Fig.6). The theory finally predicts the magnitude of the piezoresistance in response to strain (Fig.10). Eq.22 thus provides a quantitative model for designing touch sensitive materials. It allows calibrating sensors by inferring strain from resistance measurements. Sensors reading the amplitude of transient spikes would have a quasi-instantaneous rise time unlike existing sensors whose response time is limited by viscoelastic relaxation. By modelling the piezoresistance under different V_0 in Fig.10, we have shown that materials with the largest possible band offset would have the highest sensitivity to strain. By plotting the piezoresistance of HOPG/PDMS systems as a function of strain, our theory estimates a band offset of 300meV. This is consistent with the band offset obtained from thermo-activated transport in HOPG/PDMS composites [4].

The model disagrees with the experiment in the initial stages of the resistance recovery where the experimental resistance decays faster than the model (Fig.1(a)). This mismatch is believed to arise from the assumption that the connectivity of the network is unchanged by stress. This assumption is most likely to be challenged when the network is in its most metastable state near the resistance peaks.

VI. CONCLUSION

In summary, we have obtained a simple model which describes many of the experimental features of the piezoresistance of tunneling-percolation networks. This model depends of only four material parameters which may be fitted from the experimental data. This model may be used to guide the choice of material systems for touch sensitive sensors and allow modelling the properties of polymer/nanoparticle composites which are increasingly important in flexible electronics.

VII. ACKNOWLEDGEMENTS

This work has been supported by DSTL under grants CDE 32154 and CDE 28143 and an EPSRC DTP studentship (ITH).

[1] I. Balberg, J. Appl. Phys. D **42**, 064003 (2009).
[2] Y. Yaping, F. Zhang, C.-A. Di, and D. Zhu, Mater. Horiz. **2**, 140 (2015).
[3] S. Vionnet-Menot, C. Grimaldi, T. Maeder, S. Strassler, and P. Ryser, Phys.Rev.B **71**, 064201 (2005).
[4] S. Littlejohn, A. Nogaret, and S. Crampin, Adv. Mat. **23**, 2815 (2011).
[5] C. Grimaldi and I. Balberg, Phys.Rev.Lett. **96**, 066602 (2006).
[6] N. Johner, P. Ryser, C. Grimaldi, and I. Balberg, Phys.Rev.B **75**, 104204 (2007).
[7] P. M. Kogut and J. P. Straley, J. Phys. C **12**, 2151 (1979).
[8] R. Magier and D. J. Bergman, Phys.Rev.B **77**, 144406 (2008).
[9] J. G. Meier, J. W. Mani, and M. Kluppel, Phys.Rev.B **75**, 054202 (2007).
[10] S. Littlejohn, A. Nogaret, G. M. Prentice, and G. D. Pantos, Adv. Func. Mat. **23**, 5398 (2013).
[11] H. Liu et al., Nanoscale **8**, 12977 (2016).
[12] L. Chen, G. H. Chen, and L. Lu, Adv. Func. Mat. **17**, 898 (2007).
[13] R. Martin Negri et al., J.Appl.Phys. **107**, 113703 (2010).
[14] R. Zhang, M. Baxendale, and T. Peijs, Phys.Rev.B **76**, 195433 (2007).
[15] T. Someya et al., Proc. Nat. Acad. Sci. **101**, 9966 (2004).
[16] A. Chauhan, I. Taylor-Harrod, S. Littlejohn, and A. Nogaret, Nanoscale **9**, 4544 (2017).
[17] D. J. Lipomi et al., Nature Nanotech **6**, 788 (2011).
[18] C. S. Boland et al., ACS Nano **8**, 8819 (2014).
[19] C. Pang et al., Nature Mat. **11**, 795 (2012).
[20] S. C. B. Mannsfeld et al., Mature Mat. **9**, 859 (2010).
[21] D. A. G. Bruggeman, Ann. Phys. (Leipzig) **24**, 636 (1935).
[22] R. Landauer, J.Appl.Phys. **23**, 779 (1952).
[23] D. C. Pham and S. Torquato, J.Appl.Phys. **94**, 6591 (2003).
[24] M. Sahimi, B. D. Hughes, L. E. Scriven, and H. T. Davis, Phys.Rev.B **28**, 307 (1983).

[25] F. Thiel and I. M. Sokolov, Phys.Rev.E **94**, 012135 (2016).
[26] D. J. Bergman and D. Stroud, Solid State Phys. **46**, 147 (1992).
[27] D.-H. Kim et al., Science **320**, 507 (2008).
[28] D.-Y. Khang, H. Jiang, Y. Huang, and J. A. Rogers, Science **311**, 208 (2006).
[29] M. Ohring, *Material Science of Thin Films*, Academic Press, 2002.
[30] S. C. Hunter, *Mechanics of continuous media*, John Wiley, 1976.
[31] S. Torquato, B. Lu, and J. Rubinstein, Phys. Rev. A **41**, 2059 (1990).
[32] B. Lu and S. Torquato, Phys. Rev. A **41**, 5530 (1992).
[33] J. G. Simmons, J.Appl.Phys. **34**, 238 (1963).
[34] J. G. Simmons, J.Appl.Phys. **34**, 1793 (1963).
[35] A. Dehe, K. Fricke, K. Mutamba, and H. L. Hartnagel, J. Micromechanics and Microengineering **5**, 139 (1995).
[36] A. A. Barlian, W. T. Park, J. R. Mallon, A. J. Rastegar, and B. L. Pruitt, Proc. IEEE **97**, 513 (2009).
[37] E. Ungersboeck et al., IEEE Trans. Elec. Dev. **54**, 2183 (2007).
[38] J. H. Lee et al., Nanolett. **16**, 6738 (2016).